ROYAL SOCIETY OF CHEMISTRY

Check for updates

Reticular synthesis of 8-connected carboxyl hydrogen-bonded organic frameworks for white-light-emission†

Xiao-Juan Xi,[a] Yang Li,[b] Feifan Lang,[b] Jiandong Pang [ID] *[b] and Xian-He Bu [ID] *[ab]

The rational design and construction of hydrogen-bonded organic frameworks (HOFs) are crucial for enabling their practical applications, but controlling their structure and preparation as intended remains challenging. Inspired by reticular chemistry, two novel blue-emitting NKM−HOF−1 and NKM−HOF−2 were successfully constructed based on two judiciously designed peripherally extended pentiptycene carboxylic acids, namely $H_8PEP-OBu$ and $H_8PEP-OMe$, respectively. The large pores within these two HOFs can adsorb fluorescent molecules such as diketopyrrolopyrole (DPP) and 9-anthraldehyde (AnC) to form HOFs ⊃ DPP/AnC composites, subsequently used in the fabrication of white-light-emitting devices (WLEDs). Specifically, two WLEDs were assembled by coating NKM−HOF−1 ⊃ DPP-0.13/AnC-3.5 and NKM−HOF−2 ⊃ DPP-0.12/AnC-3 on a 330 nm ultraviolet LED bulb, respectively. The corresponding CIE coordinates were (0.29, 0.33) and (0.32, 0.34), along with corresponding color temperatures of 7815 K and 6073 K. This work effectively demonstrates the feasibility of employing reticular chemistry strategies to predict and design HOFs with specific topologies for targeted applications.

Introduction

Hydrogen-bonded organic frameworks (HOFs) have recently gained significant attention owing to their relatively mild preparation conditions, high crystallinity, good solution processability, and easy regeneration/recyclability.[1,2] These materials also show promising potential for diverse applications in gas adsorption and separation,[3–5] proton conduction,[6–8] catalysis,[9–11] fluorescence detection,[12–14] and biomedicine.[15–17] Over the past decade, the development in this field has brought considerable progress in utilizing different hydrogen-bonded units for constructing HOFs, such as carboxylic acid,[18–20] 2,4-diaminotriazine,[21–23] imidazole,[24–26] imidazolone,[27,28] pyrazole,[29,30] pyridine,[31–33] tetrazole,[34] cyano,[35,36] hydroxyl,[37,38] sulfonate,[39–41] and aldehyde groups.[42,43] However, hydrogen bonds are more reversible, flexible, and less directional in contrast to covalent and coordination bonds. Slight changes in ligands may have a dramatic impact on the structures and properties of HOFs.[44] This lack of directionality poses

a challenge in the precise construction of HOFs with desired structures and functionalities.

Reticular chemistry has proven to be a powerful tool not only for guiding the synthesis of various framework materials with different topologies, but also for tuning the pore properties *via* specific modification of their building units, for achieving special functionalities to meet the needs of practical applications.[45,46] A series of important advances have been made in applying reticular chemistry to the synthesis of metal–organic frameworks (MOFs) and covalent organic frameworks (COFs).[47–49] However, the study of reticular chemistry in HOFs is still in its infancy, mainly focusing on the synthesis of HOFs with the same topology by applying the shape matching π–π stacking strategy to ligands with large fused rings.[44] For example, Cao *et al.* constructed PFC-1 with sql topology based on 1,3,6,8-tetrakis(*p*-benzoic acid)pyrene (H_4TBAPy).[50,51] Farha *et al.* prepared a series of HOFs (HOF-102, HOF-101, and HOF-100) with sql topology based on pyrene-based ligands with different length side groups (carboxyl, carboxyphenyl, and carboxynaphthyl). Among them, HOF-101 is equivalent to PFC-1.[52] After this, they successfully prepared three isostructural HOFs (HOF-101-CH_3, HOF-101-NH_2, and HOF-101-F) with sql topology by modifying the carboxyphenyl group with additional functional groups (CH_3, NH_2, and F) without changing the pyrene core.[53] Hisaki *et al.* built three isostructural HOFs (C2N6DBC-1, C1N5DBC-1, and C1N4DBC-1) with dia topology using dibenzo[*g,p*]chrysene-based ligands that possess 2,6-, 1,5- and 1,4-substituted carboxynaphthyl groups, respectively.[54] Building upon these achievements, we intend to further expand

[a]College of Chemistry, State Key Laboratory of Elemento-Organic Chemistry, Nankai University, Tianjin 300071, P. R. China. E-mail: buxh@nankai.edu.cn

[b]School of Materials Science and Engineering, Smart Sensing Interdisciplinary Science Center, TKL of Metal and Molecule-Based Material Chemistry, Collaborative Innovation Center of Chemical Science and Engineering, Nankai University, Tianjin 300350, P. R. China. E-mail: jdpang@nankai.edu.cn

the application of reticular chemistry in the field of HOFs. Carboxylic acids are selected as ligands to carry out our research, since they can form directional hydrogen-bonded carboxyl dimers.[55] Previous studies have demonstrated interesting results that can guide our research. Aromatic tricarboxylic acids with C_3-symmetry can act as 3-connected (3-c) nodes to form (6, 3)-c hexagonal networks[56–58] or (10, 3)-b networks.[59] The near-planar aromatic tetracarboxylic acids can act as 4-c square nodes to form sql-[60–62] or nbo-[63] topological networks, while non-planar aromatic tetracarboxylic acids can act as 4-c tetrahedral nodes to from dia-topological networks.[64–66] In addition, non-planar aromatic tetracarboxylic acids can also form a $ThSi_2$-topological network.[67] Near-planar C_3 or C_6 symmetric aromatic hexacarboxylic acids can act as (3, 6)-c hexagonal nodes to form networks with acs topology,[70–72] or as 6-c octahedral nodes to form the pcu topology.[73] Porous HOFs based on rigid carboxylic acid above 6-c remain absent due to synthetic challenges. Therefore, our intention is to analyze the topological elements of related MOFs and then extend them to HOFs based on reticular chemistry, hoping to achieve a breakthrough in the connection number of carboxylic-acid-based HOFs as well as constructing new HOFs in a directional manner.

We first carefully analyzed the topological structure of MOF-235.[68] The trinuclear Fe_3 clusters (Scheme 1a) can be simplified as 6-c trigonal-prism nodes (Scheme 1f), and 1,4-terephthalate (Scheme 1b) can act as linear linkers (Scheme 1g) to construct

an acs-topological framework (Scheme 1e). Similar results were observed in PETHOF-1 and PETHOF-2 reported by Stoddart *et al.*[70] These two HOFs based on acs topology are constructed from the 6-c peripherally extended triptycene hexacarboxylic acid H_6PET (Scheme 1j). The H_6PET ligands are similar to the Fe_3 clusters in MOF-235 which act as 6-c trigonal-prism nodes, where the hydrogen-bonded carboxyl dimers (Scheme 1k) can be considered as the linear linker of 1,4-terephthalate in MOF-235. Similar results were also observed in ZJU–HOF–1 based on acs topology reported by Chen *et al.*[71] Stepping further, in PCN-700,[69,74] the Zr_6 clusters (Scheme 1d) can be simplified as 8-c cube nodes (Scheme 1h), and Me_2-BPDC (2,2′-dimethylbiphenyl-4,4′-dicarboxylate) (Scheme 1c) act as linear linkers to construct a bcu topology (Scheme 1i). Based on reticular chemistry, these peripherally extended pentiptycene ligands (Scheme 1l) have high potential for acting as 8-c quadrangular-prism nodes[75,76] for HOFs, and we postulate that the HOFs of bcu topology could be directionally constructed.

Herein, we undertook the design and synthesis of two peripherally extended pentiptycene ligands, namely H_8PEP-OBu (Scheme S1†) and H_8PEP-OMe (Scheme S2†). These ligands were connected through hydrogen-bonded carboxyl dimers and further assembled into NKM–HOF–1 and NKM–HOF–2 with 2-fold interpenetrated bcu topologies, assisted by weak interactions such as C–H···π between the ligands and the solvent molecules (methyl benzoate, MB). Notably, this work represents the first successful construction of porous HOFs based on rigid
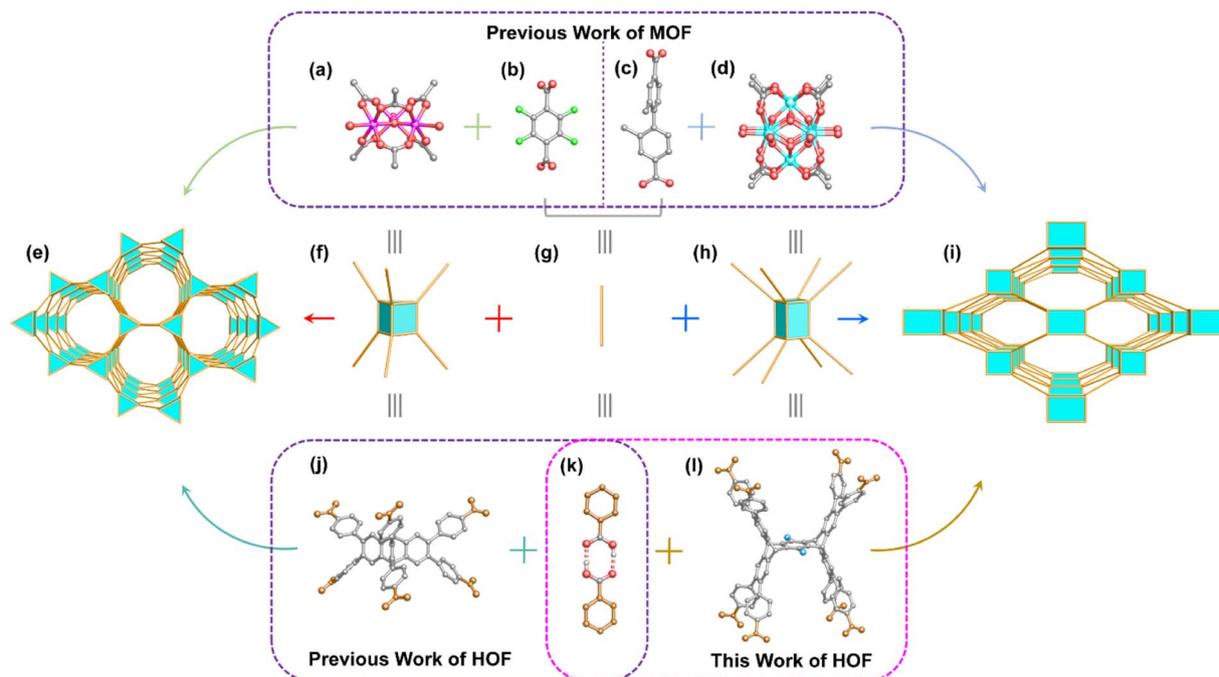
Scheme 1 Syntheses of novel HOFs inspired by reticular chemistry. (a) The Fe_3 cluster[68] in MOF-235. (b) The 1,4-terephthalate ligand in MOF-235. (c) The Me_2-BPDC ligand in PCN-700.[69] (d) The Zr_6 cluster in PCN-700. (e) Frameworks with acs topology. (f) The simplified 6-c trigonal prismatic nodes. (g) The simplified linear linkers. (h) The simplified 8-c quadrangular prism nodes. (i) Frameworks with bcu topology. (j) Peripherally extended trigonal prismatic triptycene H_6PET.[70] The brown spheres represent carboxyl groups. (k) Illustration of hydrogen-bonded carboxyl dimers. The brown spheres represent benzene rings. (l) Peripherally extended quadrangular prism pentiptycene carboxylic acid derivatives in this work. The brown spheres represent carboxyl groups, and the blue spheres represent the groups of OBu or OMe. Color legend: pink sphere, Fe; turquoise sphere, Zr; bright green sphere, F; red sphere, O; gray sphere, C.

8-c carboxylic acids. Considering the blue emission and the pore size of NKM–HOF–1 (7.8×11.6 Å^2) and NKM–HOF–2 (8.4×16.2 Å^2), two dye molecules 3,6-di(2-thienyl) diketopyrrolopyrrole (DPP) ($14.5 \times 8.1 \times 3.6$ Å^3, yellow emitting) and anthracene carboxaldehyde (AnC) ($11.6 \times 8.5 \times 3.2$ Å^3, greenish yellow emitting) were selected to adjust the luminescence properties of these HOFs. Two white light-emitting (WLE) composites NKM–HOF–1 ⊃ DPP-0.13/AnC-3.5 and NKM–HOF–2 ⊃ DPP-0.12/AnC-3 were successfully obtained by adjusting the soaking concentration of dyes. After coating them on 330 nm ultraviolet (UV) LEDs, we assembled two white-light-emitting devices (WLEDs) with CIE coordinates of (0.29, 0.33) and (0.32, 0.34), as well as color correlated temperatures (CCT) of 7815 K and 6073 K, respectively.

Results and discussion

Two D_{2h}-symmetric quadrangular-prism-shaped molecules, 6,13-dibutoxy-2,3,9,10,18,19,24,25-octa(4′-carboxyphenyl)pentiptycene (H$_8$PEP-OBu) and 6,13-dimethoxy-2,3,9,10,18,19,24,25-octa(4′-carboxyphenyl)pentiptycene (H$_8$PEP-OMe), were obtained through the multi-step syntheses according to Scheme S1 and S2.† Solvothermal reactions of H$_8$PEP-OBu or H$_8$PEP-OMe in a mixture of tetrahydrofuran and methyl benzoate (MB) at 80 °C for 3 days afforded two isostructural HOFs (namely NKM–HOF–1 and NKM–HOF–2). Single-crystal X-ray diffraction (SCXRD) analysis revealed that both NKM–HOF–1 and NKM–HOF–2 crystallize in the

orthorhombic *Pnma* space group with half of the molecule as the asymmetric unit. Therefore, similar unit-cell parameters are observed for NKM–HOF–1 ($a = 18.334$ Å, $b = 25.967$ Å, and $c = 37.965$ Å) and NKM–HOF–2 ($a = 18.397$ Å, $b = 26.378$ Å, and $c = 37.731$ Å) (Table S1†), and their analogous formulae are determined to be (H$_8$PEP-OBu)(MB)$_3$ and (H$_8$PEP-OMe)(MB)$_3$, respectively. Herein, only NKM–HOF–1 is particularly discussed in detail, and the corresponding crystal structure information of NKM–HOF–2 is shown in Fig. S1, S2 and S3.† In the three-dimensional (3D) supramolecular framework of NKM–HOF–1 (Fig. 1a), each 8-c quadrangular prism H$_8$PEP-OBu ligand is connected with eight neighboring H$_8$PEP-OBu ligands (Fig. S2a†) through eight pairs of O–H···O hydrogen bonds between –COOH groups (O···H distance ranging between 1.737–1.807 Å, O···O distance ranging between 2.573–2.637 Å, and O–H···O bond angle ranging between 166.8–173.3°) (Table S2†). Evidence for the formation of these O–H···O hydrogen bonds can also be observed in the electrostatic potential (ESP) diagram of NKM–HOF–1 (Fig. S4†), revealing that the negative potential areas are primarily located on the carbonyl oxygen atoms of eight carboxyl groups, while the positive potential areas are primarily located on the hydroxyl hydrogen atoms of eight carboxyl groups. This facilitates the donor–acceptor interaction between carboxyl groups, thus promoting the formation of hydrogen-bonded carboxyl dimers during the crystallization process. The resulting single-set of supramolecular networks with bcu topology exhibits large porosity that enables the assembly of a second set in its voids, thereby
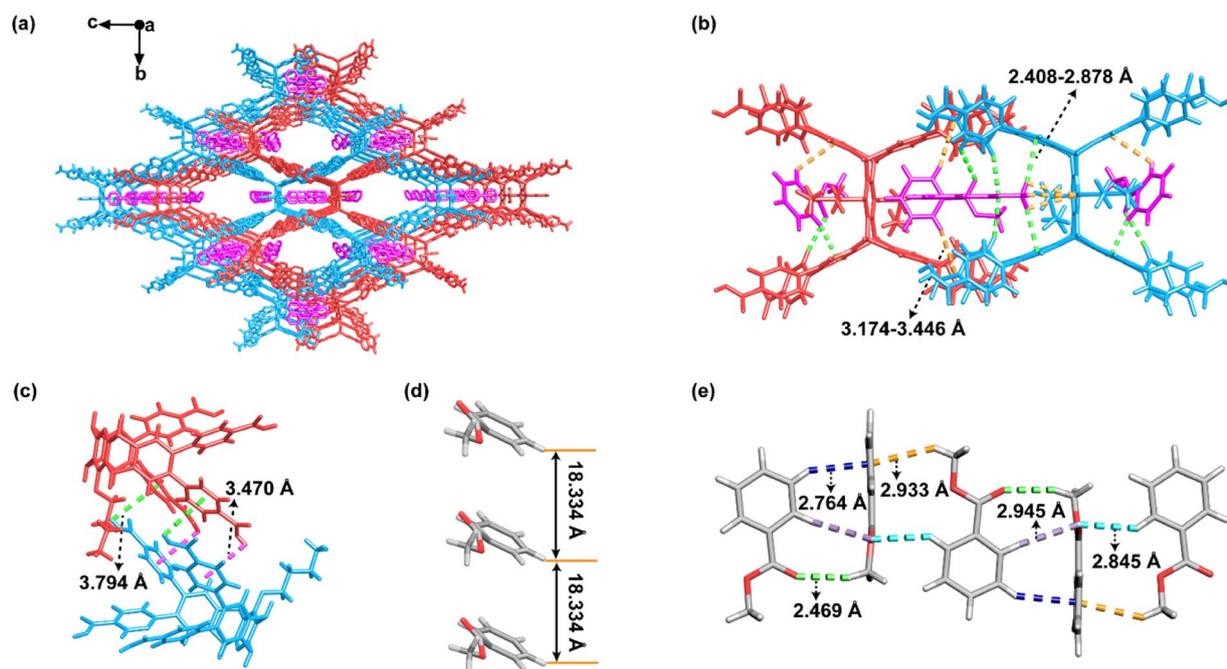

Fig. 1 (a) SCXRD structure of NKM–HOF–1 showing its 2-fold interpenetrated 3D supramolecular framework. Two sets of independent networks are plotted in red and light blue. The pores are filled with two types of MB molecules, which are plotted in pink. H atoms are omitted for clarity. (b) Illustration of the multiple C–H···π interactions formed among MB molecules and adjacent H$_8$PEP-OBu molecules (green dotted lines: stronger interactions; cyan dotted lines: weaker interactions). (c) Illustration of the multiple C–H···π interactions between adjacent H$_8$PEP-OBu molecules. (d) The parallelly arranged MB molecules in the large pores of NKM–HOF–1. (e) The MB molecules packed in a –[A–B–C–D]– manner in the small pores of NKM–HOF–1.

stabilizing the entire architecture. The two adjacent 3D frameworks form a 2-fold interpenetrated structure through the C–H···π interaction between the H_8PEP-OBu ligands (H···π distance of 3.470 or 3.794 Å) (Fig. 1c) and the C–H···π interaction between the ligands and the MB molecules (distances for strong H···π ranging between 2.408–2.878 Å and for weak H···π ranging between 3.174–3.446 Å) (Fig. 1b). There are two types of MB molecules in the structure, as shown in Fig. 1a. The adjacent MB molecules in the large pores are arranged in a –[A–A]– manner along the a-axis with a distance of 18.334 Å without any intermolecular interaction (Fig. 1d). Conversely, the adjacent MB molecules in the small pores form a 1D chain via C–H···O hydrogen bonds (H···O distances ranging between 2.469–2.945 Å) in a –[A–B–C–D]– manner along the a-axis (Fig. 1e). The MB molecules surely play a pivotal role in the templating of the assembly process, as the attempted syntheses without involving MB yielded no crystals. As shown in Fig. S5,† after removing the solvent molecules, NKM–HOF–1 shows 2D cage-like pores with a hexagonal window measuring 7.8 × 11.6 Å² in size and an abnormal hexagonal window measuring 1.9 × 5.0 Å² in size along the a-axis. These cage-like pores also have an extremely narrow quadrilateral window with a size of 0.2 × 15.1 Å² along the b-axis (Fig. S5c†).

According to the analysis using ToposPro,[77,78] the network topology of NKM–HOF–1 exhibits a class IIa interpenetration, where two networks are related by a symmetric center.[70] In the framework of NKM–HOF–1, each H_8PEP-OBu molecule can be simplified as an 8-c node (Fig. 2a and d), rendering an 8-c bcu net topology with a $(4^{24}.6^4)$ point symbol (Fig. 2c and f). As shown in Fig. 2b and e, the 8-c bcu net of NKM–HOF–1 consists of two hexagonal windows along the a-axis (18.3 × 38.0 Å²) and along the b-axis (26.0 × 38.0 Å²). One individual network possesses pores with a large and suitable configuration, further resulting in two of such identical frameworks interpenetrated along the b-axis through these quadrilateral windows (Fig. 2c and f). The total guest-accessible void space in NKM–HOF–1 (64.5%) calculated with a probe radius of 1.2 Å in PLATON software[79] is slightly smaller than that of NKM–HOF–2 (68.6%), which is consistent with the difference in pore size (Fig. S5†).

The phase purity of the as-synthesized NKM–HOF–1 and NKM–HOF–2 was confirmed by powder X-ray diffraction (PXRD) (Fig. S6†). Thermogravimetric analysis (TGA) found that NKM–HOF–1 and NKM–HOF–2 were both stable up to about 350 °C (Fig. S7†). The N_2 adsorption and desorption isotherms at 77 K show that there is almost no N_2 adsorption for activated NKM–HOF–1 and NKM–HOF–2 using supercritical CO_2 activation (Fig. S8†), indicating the collapse of the frameworks after desolvation. Fresh crystals of both HOFs were finally dissolved in methanol or ethanol, but not in acetonitrile. The PXRD patterns of two HOFs after soaking in acetonitrile for 3 days remained unchanged (Fig. S6†), indicating their high stability in acetonitrile. Considering the above results, the following dye encapsulation experiments were performed with acetonitrile.

The great potential of WLEDs in solid-state light sources has attracted extensive attention.[80] Two common methods are employed to fabricate WLEDs. The first method involves integrating LED chips emitting the three primary colors (blue, green, and red), and the resulting multi-chip system is therefore complicated and expensive.[81] The alternative approach entails coating yellow-emitting phosphors onto blue-emitting LED
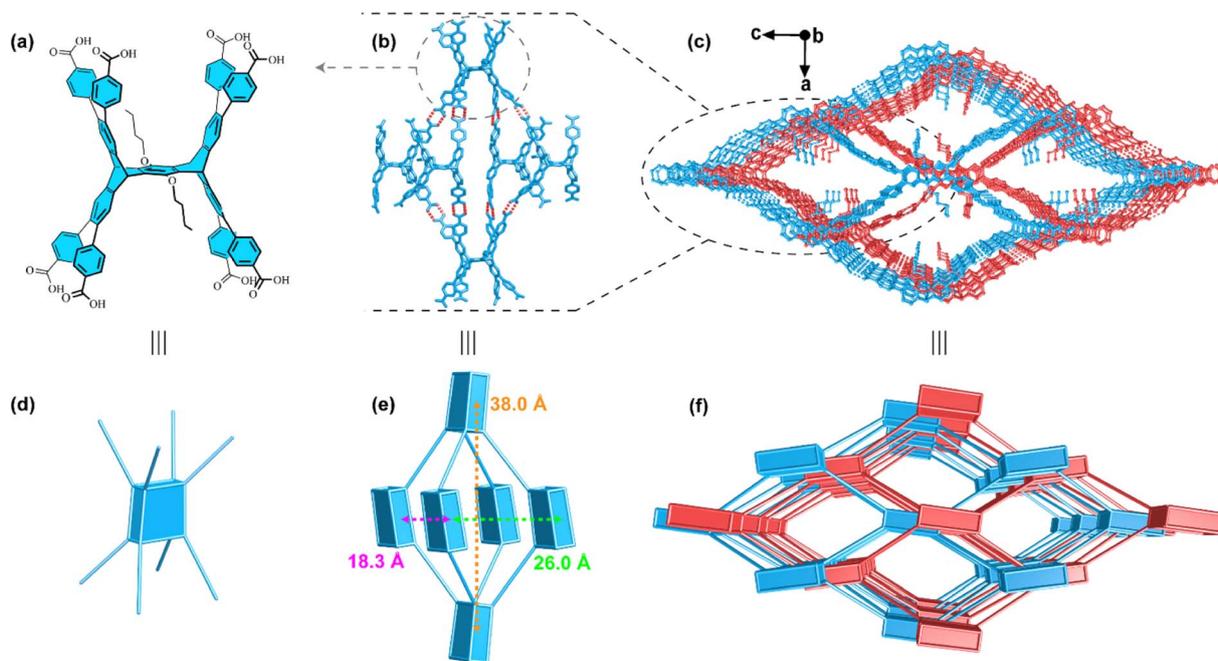

Fig. 2 (a) The structure of the ligand H_8PEP-OBu. (b) The octahedral cavities viewed from the crystal structure (red dotted lines represent H-Bonds). (c) 2-fold interpenetrated frameworks of NKM–HOF–1 (each color represents an individual bcu net). (d) The 8-c quadrangular prism nodes simplified from H_8PEP-OBu. (e) The octahedral cavities viewed from the topological structure. (f) The 2-fold interpenetrated bcu topological net of NKM–HOF–1.

chips (or white-emitting phosphors onto ultraviolet-emitting LED chips).[82] Although white-emitting phosphors can be obtained by mechanically mixing organic fluorescent dyes which emit the three primary colors or complementary colors (such as blue and yellow), the efficiency of energy transfer is hindered due to the non-uniformity of the mixing process. In addition, many organic fluorescent dyes exhibit reduced or even no emission properties in the solid state compared to their solution phase, which is due to the aggregation-caused quenching (ACQ) effects.[83] To address these drawbacks, the encapsulation of organic fluorescent dyes into porous framework materials has been explored. Such a strategy not only enhances the uniform dispersion of dyes, but also effectively mitigates the ACQ effect, which eventually leads to competent WLE behaviors. Significant progress has already been made in applying MOFs as hosts for adsorbing fluorescent dyes to construct WLE materials.[84] Notably, by sharing similar characteristics such as high structural porosity and tunability, HOFs have also emerged as promising candidates for WLE materials owing to their unique features like good solvent processability.[85,86] We observed the maximum emission wavelength of NKM–HOF–1 to be 416 nm upon excitation at an optimal wavelength of 365 nm, which was blue-shifted compared with that of amorphous $H_8PEP-OBu$ (457 nm), which is presumably due to a certain level of structural rigidity gained after the framework assembly (Fig. S9†). The photoluminescence (PL) quantum yield of NKM–HOF–1 was 18.6%, and its CIE coordinates were (0.16, 0.08) (Fig. S10†). Similarly, at an optimal excitation wavelength of 365 nm, the maximum emission wavelength of NKM–HOF–2 was 414 nm, which was also blue-shifted compared with that of amorphous $H_8PEP-OMe$ molecules (455 nm). The PL quantum yield of NKM–HOF–2 was 19.9%, and its CIE coordinates were (0.16, 0.08).

Considering the blue emission characteristics of both NKM–HOF–1 and NKM–HOF–2, two fluorescent molecules, 3,6-di(2-thienyl)diketopyrrolopyrrole (DPP) which emitted yellow light[87,88] and anthracene carboxaldehyde (AnC) which emitted greenish yellow light[89] were chosen as the introduced guest luminescence units to achieve WLE. As shown in Fig. S11,† the molecular sizes of DPP and AnC are $14.5 \times 8.1 \times 3.6$ Å^3 and $11.6 \times 8.5 \times 3.2$ Å^3, respectively, which are both comparable to the dimensions of the hexagonal windows in NKM–HOF–1 (7.8×11.6 Å^2) and NKM–HOF–2 (8.4×16.2 Å^2).[90] The PXRD patterns of NKM-HOF ⊃ DPP/AnC are all in agreement with that of pristine NKM–HOF–1 and NKM–HOF–2, respectively, indicating that the guest molecules encapsulated in the pores did not destroy the crystal structure (Fig. S6†). In order to cover the entire emission wavelength range, excitation light of 330 nm was utilized in fluorescence spectroscopy for studying the WLE behaviors (Fig. S12†). First, the acetonitrile solutions of pure DPP (0.12 mmol L^{-1}) and pure AnC (3.80 mmol L^{-1}) respectively exhibited double yellow emissions (around 535 nm and 572 nm) and a single greenish-yellow emission (around 470 nm) upon irradiation (Fig. S13†). Next, we obtained two host-guest composites of NKM–HOF–1 ⊃ DPP-0.12 and NKM–HOF–1 ⊃ DPP-0.25 by immersing the crystals of NKM–HOF–1 into the acetonitrile solution of DPP (0.12 mmol L^{-1} and 0.25 mmol L^{-1})

at 50 °C for 24 h. The TGA curve showed that the total weight loss of NKM-HOFs ⊃ DPP/AnC is larger than that of activated NKM-HOFs (Fig. S7†), indicating the successful introduction of the dye molecules. Furthermore, Fourier transform infrared (FTIR) spectra showed that all characteristic absorptions in DPP and AnC were observed in the spectrum of NKM–HOF–1 ⊃ DPP/AnC, and the peaks at 1709, 1511, and 1411 cm^{-1} were significantly enhanced, which can be attributed to the contribution of C=O stretching vibration of DPP and AnC, the amide II band of DPP, and the thiophene ring of DPP, respectively (Fig. S14†). Similarly, the peaks of NKM–HOF–2 ⊃ DPP/AnC at 1705, 1507, and 1398 cm^{-1} were also significantly enhanced owing to the contribution of DPP and AnC. The adsorption of AnC can also be demonstrated by using the ^{1}H-NMR spectra of NKM-HOFs ⊃ DPP/AnC (Fig. S15 and S16†). The lack of DPP characteristic peaks is due to the relatively weak intensity of DPP characteristic peaks in DMSO-d_6 (caused by the poor solubility of DPP in DMSO-d_6, Fig. S17†) and the small amount of DPP adsorbed on NKM-HOFs ⊃ DPP/AnC. However, the successful introduction of DPP can be proved by using the energy dispersive spectroscopy mapping (EDS-mapping) images, which shows that the S and N elements belonging to DPP are uniformly distributed in the crystals of NKM-HOFs ⊃ DPP/AnC (Fig. S18 and S19†). In addition, the recovered NKM-HOFs (NKM-HOFs ⊃ DPP/AnC were activated with acetonitrile at 60 °C for 4 days, and the acetonitrile was replaced three times a day) are still pink (Fig. S20†), which further indicates that the dye molecules entered the channels of the NKM-HOFs rather than simply being adsorbed on the surface.

Under 330 nm excitation, the emission peaks corresponding to NKM–HOF–1 and DPP, respectively, are shown at 409 nm and 548/588 nm in both NKM–HOF–1 ⊃ DPP-0.12 and NKM–HOF–1 ⊃ DPP-0.25 samples. It was clearly observed that the former was blue-shifted compared to that of pure NKM–HOF–1 (416 nm) and the latter was red-shifted compared to that in the pure DPP molecules (535/572 nm), indicating that the energy transfer from NKM–HOF–1 to DPP occurs.[91] The CIE coordinates of NKM–HOF–1 ⊃ DPP-0.12 (0.24, 0.16) and NKM–HOF–1 ⊃ DPP-0.25 (0.25, 0.18) are located in the blue-purple region (Fig. S21†), which deviates from the white light point. Due to the limited solubility of DPP in acetonitrile, the content of DPP encapsulated in NKM–HOF–1 cannot be further improved by increasing the initial concentration of DPP acetonitrile solution. It can be inferred from the trend of CIE coordinates that on further increasing the amount of DPP adsorbed on the HOF, the CIE coordinates of such composites should gradually shift towards the orange-red region. Parallelly, NKM–HOF–1 ⊃ AnC-3.8 was obtained after the immersion of NKM–HOF–1 crystals in the acetonitrile solution of AnC (3.80 mmol L^{-1}) at 50 °C for 24 h. Again, under 330 nm excitation, the emission peaks corresponding to NKM–HOF–1 at 404 nm and AnC at 504 nm in NKM–HOF–1 ⊃ AnC-3.8 were blue-shifted and red-shifted compared with those of pure NKM–HOF–1 (416 nm) and AnC (470 nm), respectively, which is possibly due to the energy transfer from NKM–HOF–1 to AnC. The CIE coordinates (0.23, 0.36) of NKM–HOF–1 ⊃ AnC-3.8 are located around the cyan region. In the case of using NKM–HOF–2 as the host, the

emission spectra of NKM–HOF–2 ⊃ DPP-0.12, NKM–HOF–2 ⊃ DPP-0.25, and NKM–HOF–2 ⊃ AnC-3.8 are very similar to those of NKM–HOF–1 ⊃ DPP-0.12, NKM–HOF–1 ⊃ DPP-0.25, and NKM–HOF–1 ⊃ AnC-3.8 (Fig. S21c and d†).

Considering the abovementioned results, the simultaneous presence of DPP and AnC in NKM–HOF–1 could be a possible route towards WLE. The PL spectrum of NKM–HOF–1, and the absorption/PL spectra of pure DPP or AnC in acetonitrile are shown in Fig. S22.† There is a considerable overlap between the PL spectrum of NKM–HOF–1 and the absorption spectrum of AnC in the range of 367–460 nm, as well as between the PL spectrum of AnC and the absorption spectrum of DPP in the range of 440–650 nm, which ensures the effective transfer of energy between the HOF host and the guest dyes. NKM–HOF–1 ⊃ DPP/AnC exhibits three emission bands when excited using 330 nm UV light (Fig. 3). The first emission band Em I had a single peak at around 404 nm, which was blue-shifted compared with that of pure NKM–HOF–1 (416 nm) due to the energy transfer from NKM–HOF–1 to AnC. Em II exhibited double emission peaks at around 476 nm and 506 nm attributed to AnC, which arise from the energy transfer processes occurring from NKM–HOF–1 to AnC and subsequently from AnC to DPP, respectively. Em III also had double emission peaks at around 548 nm and 585 nm attributed to DPP, which were red-shifted compared with those of pure DPP in acetonitrile

(around 535 nm and 572 nm). By adjusting the concentration of AnC within a suitable range (0.50–4.00 mmol L^{-1}) while maintaining a constant concentration of DPP at 0.13 mmol L^{-1} in the solution, the intensities of Em II and Em III for the NKM–HOF–1 ⊃ DPP/AnC composites gradually increased while those of Em I barely changed (Fig. 3a). The corresponding CIE coordinates sequentially changed from (0.24, 0.20) to (0.29, 0.36) (Fig. 3b and Table S3†). Particularly, when the concentrations of AnC and DPP in the solution were set respectively at 3.50 mmol L^{-1} and 0.13 mmol L^{-1}, the resulting CIE coordinates of the composite reached (0.29, 0.33), which is indicative of WLE. According to McCamy's relation,[92,93] the CCT was calculated to be 7815 K which was classified as 'cool white light'. Moreover, the luminescence lifetimes of NKM–HOF–1 (2.16 ns) decreased from 2.16 ns to 0.53 ns after the introduction of DPP and AnC, and the energy transfer efficiency was determined to be 75% (Table S4 and Fig. S23†).[94] The quantum yields of NKM–HOF–1 ⊃ DPP-0.13/AnC-3.5 also changed to 7.08% (Table S5†).

In the case of NKM–HOF–2, similar results were obtained on adjusting the concentration of AnC (0.50–4.00 mmol L^{-1}) while maintaining the concentration of DPP at 0.12 mmol L^{-1} during the encapsulation. The intensities of Em II and Em III for NKM–HOF–2 ⊃ DPP/AnC composites gradually increased while those of Em I hardly changed (Fig. 3c), accompanied by their CIE coordinates changing from (0.26, 0.21) to (0.32, 0.36) (Fig. 3d and Table S6†). The optimized concentrations of AnC and DPP in solution were 3.00 mmol L^{-1} and 0.12 mmol L^{-1}, leading to the CIE coordinates of (0.32, 0.34), indicative of WLE. The corresponding CCT is calculated to be 6073 K which represents 'cool white light'. The lifetime of NKM–HOF–2 decreased from 2.55 ns to 0.50 ns after the formation of host–guest composites and the energy transfer efficiency was 80%. The quantum yields of NKM–HOF–2 ⊃ DPP-0.12/AnC-3 were 8.71%. These results further emphasize the energy transfer between HOFs and dye molecules.

In addition to the successful encapsulation and fine-tuning of dye molecules within NKM–HOF–1 and NKM–HOF–2, these HOF ⊃ dye composites have also been demonstrated to be suitable candidates for practical WLE applications through the fabrication of WLED devices. We prepared these bulbs by simply coating NKM–HOF–1 ⊃ DPP-0.13/AnC-3.5 or NKM–HOF–2 ⊃ DPP-0.12/AnC-3 onto commercially available 330 nm ultraviolet LED bulbs. The resulting WLEDs emitted bright white light at a voltage of 4.5–6.5 V and current of 350 mA, as shown in Fig. 3. These results strongly support the promising potential of NKM-HOF ⊃ dyes as novel WLE materials for a wide range of practical white lighting applications.

Fig. 3 (a) Normalized PL spectra and (b) corresponding CIE coordinates of NKM–HOF–1 treated with acetonitrile solutions containing a constant concentration of DPP (0.13 mmol L^{-1}) but different concentrations of AnC (0.5–4 mmol L^{-1}). Inset of (b) shows the photographs of a 330 nm ultraviolet LED when turned off (left), when coated with NKM–HOF–1 ⊃ DPP-0.13/AnC-3.5 and turned off (middle), and wh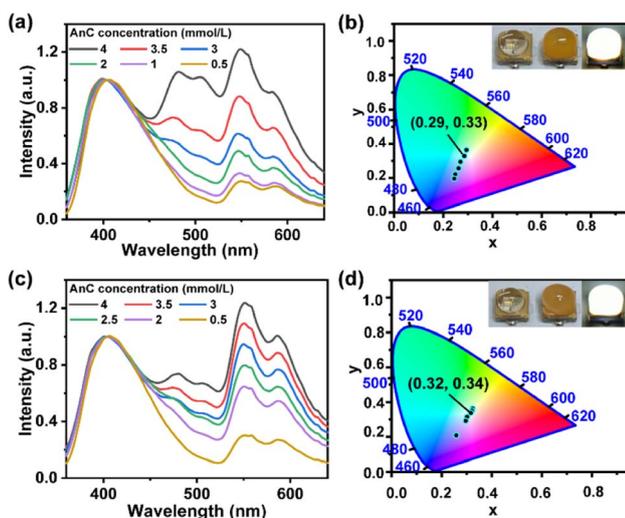en coated with NKM–HOF–1 ⊃ DPP-0.13/AnC-3.5 and turned on (right). (c) Normalized PL spectra and (d) corresponding CIE coordinates of NKM–HOF–2 treated with acetonitrile solutions containing a constant concentration of DPP (0.12 mmol L^{-1}) but different concentrations of AnC (0.5–4 mmol L^{-1}). Inset of (d) shows the photographs of a 330 nm ultraviolet LED when turned off (left), when coated with NKM–HOF–2 ⊃ DPP-0.12/AnC-3 and turned off (middle), and when coated with NKM–HOF–2 ⊃ DPP-0.12/AnC-3 and turned on (right).

Conclusions

In conclusion, the effective application and extension of reticular chemistry in the construction of novel HOFs have allowed for the precise control of their structures and properties. We have directionally constructed two new HOF materials, NKM–HOF–1 and NKM–HOF–2, with a record-high topology connection number based on two 8-c prismatic pentiptycene carboxylic acids (H$_8$PEP-OBu and H$_8$PEP-OMe). The large pore sizes of

NKM–HOF–1 (7.8×11.6 Å^2) and NKM–HOF–2 (8.4×16.2 Å^2) endow them with satisfactory ability for guest molecule encapsulation. With the successful incorporation of DPP (yellow-emitting) and AnC (greenish-yellow-emitting) into the blue-emitting NKM–HOF–1 and NKM–HOF–2, NKM–HOF–1 ⊃ DPP-0.13/AnC-3.5 and NKM–HOF–2 ⊃ DPP-0.12/AnC-3 could be obtained *via* the subtle tuning of the contents of the two dyes. These two optimized WLE composites demonstrated their versatility and potential applications in WLEDs, achieving CIE coordinates of (0.29, 0.33) and (0.32, 0.34), as well as a CCT of 7815 K and 6073 K. This work highlights the immense possibilities that reticular chemistry offers in the design of new structures and the enhancement of properties in HOFs, and we can expect that such a strategy would lead to further advancements in this field.

Data availability

The authors confirm that the data supporting the findings of this study are available within the article [and/or its ESI†].

Author contributions

X.-J. Xi, J. Pang, and X.-H. Bu conceived and designed the experiment. X.-J. Xi performed the synthesis and characterization of the material, and wrote the original draft of the manuscript. Y. Li contributed to the synthesis and a part of characterization experiments. F. Lang, J. Pang, and X.-H. Bu reviewed and revised this manuscript.

Conflicts of interest

The authors declare no competing interests.

Acknowledgements

Notes and references

1 L. Chen, B. Zhang, L. Chen, H. Liu, Y. Hu and S. Qiao, *Adv. Mater.*, 2022, **3**, 3680–3708.

2 R.-B. Lin, Y. He, P. Li, H. Wang, W. Zhou and B. Chen, *Chem. Soc. Rev.*, 2019, **48**, 1362–1389.

3 Y. Cai, J. Gao, J.-H. Li, P. Liu, Y. Zheng, W. Zhou, H. Wu, L. Li, R.-B. Lin and B. Chen, *Angew. Chem., Int. Ed.*, 2023, **62**, e202308579.

4 Y. Zhou, C. Chen, R. Krishna, Z. Ji, D. Yuan and M. Wu, *Angew. Chem., Int. Ed.*, 2023, **62**, e202305041.

5 Z. Zhang, Y. Ye, S. Xiang and B. Chen, *Acc. Chem. Res.*, 2022, **55**, 3752–3766.

6 S. Chen, Y. Ju, H. Zhang, Y. Zou, S. Lin, Y. Li, S. Wang, E. Ma, W. Deng, S. Xiang, B. Chen and Z. Zhang, *Angew. Chem., Int. Ed.*, 2023, **62**, e202308418.

7 Y. Sun, J. Wei, Z. Fu, M. Zhang, S. Zhao, G. Xu, C. Li, J. Zhang and T. Zhou, *Adv. Mater.*, 2023, **35**, 2208625.

8 S. C. Pal, D. Mukherjee, R. Sahoo, S. Mondal and M. C. Das, *ACS Energy Lett.*, 2021, **6**, 4431–4453.

9 C. Huang, C. Zhao, Q. Deng, H. Zhang, D. Yu, J. Ren and X. Qu, *Nat. Catal.*, 2023, **6**, 729–739.

10 L. Tong, Y. Lin, X. Kou, Y. Shen, Y. Shen, S. Huang, F. Zhu, G. Chen and G. Ouyang, *Angew. Chem., Int. Ed.*, 2023, **62**, e202218661.

11 C. Wang, X. Song, Y. Wang, R. Xu, X. Gao, C. Shang, P. Lei, Q. Zeng, Y. Zhou, B. Chen and P. Li, *Angew. Chem., Int. Ed.*, 2023, **62**, e202311482.

12 B. Wang, R.-B. Lin, Z. Zhang, S. Xiang and B. Chen, *J. Am. Chem. Soc.*, 2020, **142**, 14399–14416.

13 P.-D. Liu, A.-G. Liu, P.-M. Wang, Y. Chen and B. Li, *Chin. J. Struct. Chem.*, 2023, **42**, 100001.

14 Z. Ke, K. Chen, Z. Li, J. Huang, Z. Yao, W. Dai, X. Wang, C. Liu, S. Xiang and Z. Zhang, *Chin. Chem. Lett.*, 2021, **32**, 3109–3112.

15 H. Zhang, D. Yu, S. Liu, C. Liu, Z. Liu, J. Ren and X. Qu, *Angew. Chem., Int. Ed.*, 2022, **61**, e202109068.

16 D. Yu, H. Zhang, Z. Liu, C. Liu, X. Du, J. Ren and X. Qu, *Angew. Chem., Int. Ed.*, 2022, **61**, e202201485.

17 G. Chen, S. Huang, X. Ma, R. He and G. Ouyang, *Nat. Protoc.*, 2023, **18**, 2032–2050.

18 M. Jiang, X. Yan, Y. Wang, F. Pu, H. Liu, Y. Li, C. Yang, J. Zhu, X. Liu, J. Ren and X. Qu, *Adv. Funct. Mater.*, 2023, **33**, 2300091.

19 X. Yu Gao, Y. Wang, E. Wu, C. Wang, B. Li, Y. Zhou, B. Chen and P. Li, *Angew. Chem., Int. Ed.*, 2023, e202312393.

20 Y.-L. Li, Q. Yin, T.-F. Liu, R. Cao and W.-B. Yuan, *Chin. J. Struct. Chem.*, 2019, **38**, 2083–2088.

21 J. Samanta, R. W. Dorn, W. Zhang, X. Jiang, M. Zhang, R. J. Staples, A. J. Rossini and C. Ke, *Chem*, 2022, **8**, 253–267.

22 I. Hisaki, C. Xin, K. Takahashi and T. Nakamura, *Angew. Chem., Int. Ed.*, 2019, **58**, 11160–11170.

23 Y. He, S. Xiang and B. Chen, *J. Am. Chem. Soc.*, 2011, **133**, 14570–14573.

24 Q. Yang, Y. Wang, Y. Shang, J. Du, J. Yin, D. Liu, Z. Kang, R. Wang, D. Sun and J. Jiang, *Cryst. Growth Des.*, 2020, **20**, 3456–3465.

25 W. Yan, X. Yu, T. Yan, D. Wu, E. Ning, Y. Qi, Y.-F. Han and Q. Li, *Chem. Commun.*, 2017, **53**, 3677–3680.

26 D.-D. Zhou, Y.-T. Xu, R.-B. Lin, Z.-W. Mo, W.-X. Zhang and J.-P. Zhang, *Chem. Commun.*, 2016, **52**, 4991–4994.

27 A. Pulido, L. Chen, T. Kaczorowski, D. Holden, M. A. Little, S. Y. Chong, B. J. Slater, D. P. McMahon, B. Bonillo, C. J. Stackhouse, A. Stephenson, C. M. Kane, R. Clowes, T. Hasell, A. I. Cooper and G. M. Day, *Nature*, 2017, **543**, 657–664.

28 M. Mastalerz and I. M. Oppel, *Angew. Chem., Int. Ed.*, 2012, **51**, 5252–5255.

29 Z. Zhang, M. I. Hashim and O. Š. Miljanić, *Chem. Commun.*, 2017, **53**, 10022–10025.

30 T.-H. Chen, I. Popov, W. Kaveevivitchai, Y.-C. Chuang, Y.-S. Chen, O. Daugulis, A. J. Jacobson and O. Š. Miljanić, *Nat. Commun.*, 2014, **5**, 5131.

31 C. A. Halliwell, S. E. Dann, J. Ferrando-Soria, F. Plasser, K. Yendall, E. V. Ramos-Fernandez, G. T. Vladisavljević, M. R. J. Elsegood and A. Fernandez, *Angew. Chem., Int. Ed.*, 2022, **61**, e202208677.

32 H. Yamagishi, H. Sato, A. Hori, Y. Sato, R. Matsuda, K. Kato and T. Aida, *Science*, 2018, **361**, 1242–1246.

33 X.-Z. Luo, X.-J. Jia, J.-H. Deng, J.-L. Zhong, H.-J. Liu, K.-J. Wang and D.-C. Zhong, *J. Am. Chem. Soc.*, 2013, **135**, 11684–11687.

34 M. I. Hashim, H. T. M. Le, T.-H. Chen, Y.-S. Chen, O. Daugulis, C.-W. Hsu, A. J. Jacobson, W. Kaveevivitchai, X. Liang, T. Makarenko, O. Š. Miljanić, I. Popovs, H. V. Tran, X. Wang, C.-H. Wu and J. I. Wu, *J. Am. Chem. Soc.*, 2018, **140**, 6014–6026.

35 Y. Shi, S. Wang, W. Tao, J. Guo, S. Xie, Y. Ding, G. Xu, C. Chen, X. Sun, Z. Zhang, Z. He, P. Wei and B. Z. Tang, *Nat. Commun.*, 2022, **13**, 1882.

36 M. C. Das, S. C. Pal and B. Chen, *Joule*, 2022, **6**, 22–27.

37 Q. Huang, W. Li, Z. Mao, H. Zhang, Y. Li, D. Ma, H. Wu, J. Zhao, Z. Yang, Y. Zhang, L. Gong, M. P. Aldred and Z. Chi, *Chem*, 2021, **7**, 1321–1332.

38 J. Sun, H.-X. Liu and T.-F. Liu, *Chin. J. Struct. Chem.*, 2021, **40**, 1082–1087.

39 A. H. Slavney, H. K. Kim, S. Tao, M. Liu, S. J. L. Billinge and J. A. Mason, *J. Am. Chem. Soc.*, 2022, **144**, 11064–11068.

40 S. Zhang, J. Fu, S. Das, K. Ye, W. Zhu and T. Ben, *Angew. Chem., Int. Ed.*, 2022, **61**, e202208660.

41 Z. Fan, S. Zheng, H. Zhang, K. Chen, Y. Li, C. Liu, S. Xiang and Z. Zhang, *Chin. Chem. Lett.*, 2022, **33**, 4317–4320.

42 L. Chen, Z. Yuan, H. Zhang, Y. Ye, Y. Yang, F. Xiang, K. Cai, S. Xiang, B. Chen and Z. Zhang, *Angew. Chem., Int. Ed.*, 2022, **61**, e202213959.

43 M.-X. Lv, S. Jiang, C. Wang, Q. Dong, F.-Y. Bai and Y.-H. Xing, *CrystEngComm*, 2022, **24**, 5442–5449.

44 Z.-J. Lin, S. A. R. Mahammed, T.-F. Liu and R. Cao, *ACS Cent. Sci.*, 2022, **8**, 1589–1608.

45 W. Gong, Y. Xie, T. D. Pham, S. Shetty, F. A. Son, K. B. Idrees, Z. Chen, H. Xie, Y. Liu, R. Q. Snurr, B. Chen, B. Alameddine, Y. Cui and O. K. Farha, *J. Am. Chem. Soc.*, 2022, **144**, 3737–3745.

46 M. Chafiq, A. Chaouiki and Y. G. Ko, *Nano-Micro Lett.*, 2023, **15**, 213.

47 Z. Chen, K. O. Kirlikovali, P. Li and O. K. Farha, *Acc. Chem. Res.*, 2022, **55**, 579–591.

48 R. Freund, O. Zaremba, G. Arnauts, R. Ameloot, G. Skorupskii, M. Dincă, A. Bavykina, J. Gascon, A. Ejsmont, J. Goscianska, M. Kalmutzki, U. Lächelt, E. Ploetz, C. S. Diercks and S. Wuttke, *Angew. Chem., Int. Ed.*, 2021, **60**, 23975–24001.

49 A. Ejsmont, J. Andreo, A. Lanza, A. Galarda, L. Macreadie, S. Wuttke, S. Canossa, E. Ploetz and J. Goscianska, *Coord. Chem. Rev.*, 2021, **430**, 213655.

50 Q. Yin, P. Zhao, R. J. Sa, G. C. Chen, J. Lu, T. F. Liu and R. Cao, *Angew. Chem., Int. Ed.*, 2018, **57**, 7691–7696.

51 W. K. Qin, D. H. Si, Q. Yin, X. Y. Gao, Q. Q. Huang, Y. N. Feng, L. Xie, S. Zhang, X. S. Huang, T. F. Liu and R. Cao, *Angew. Chem., Int. Ed.*, 2022, **61**, e202202089.

52 K. Ma, P. Li, J. H. Xin, Y. Chen, Z. Chen, S. Goswami, X. Liu, S. Kato, H. Chen, X. Zhang, J. Bai, M. C. Wasson, R. R. Maldonado, R. Q. Snurr and O. K. Farha, *Cell Rep. Phys. Sci.*, 2020, **1**, 100024.

53 Y. Wang, K. Ma, J. Bai, T. Xu, W. Han, C. Wang, Z. Chen, K. O. Kirlikovali, P. Li, J. Xiao and O. K. Farha, *Angew. Chem., Int. Ed.*, 2022, **61**, e202115956.

54 Y. Suzuki, M. Yamaguchi, R. Oketani and I. Hisaki, *Mater. Chem. Front.*, 2023, **7**, 106–116.

55 X. Song, Y. Wang, C. Wang, D. Wang, G. Zhuang, K. O. Kirlikovali, P. Li and O. K. Farha, *J. Am. Chem. Soc.*, 2022, **144**, 10663–10687.

56 Y.-L. Li, E. V. Alexandrov, Q. Yin, L. Li, Z.-B. Fang, W. Yuan, D. M. Proserpio and T.-F. Liu, *J. Am. Chem. Soc.*, 2020, **142**, 7218–7224.

57 W. Yang, W. Zhou and B. Chen, *Cryst. Growth Des.*, 2019, **19**, 5184–5188.

58 C. A. Zentner, H. W. Lai, J. T. Greenfield, R. A. Wiscons, M. Zeller, C. F. Campana, O. Talu, S. A. FitzGerald and J. L. Rowsell, *Chem. Commun.*, 2015, **51**, 11642–11645.

59 W. Yang, J. Wang, H. Wang, Z. Bao, J. C.-G. Zhao and B. Chen, *Cryst. Growth Des.*, 2017, **17**, 6132–6137.

60 T. Hashimoto, R. Oketani, M. Nobuoka, S. Seki and I. Hisaki, *Angew. Chem., Int. Ed.*, 2023, **62**, e202215836.

61 Z.-J. Lin, J.-Y. Qin, X.-P. Zhan, K. Wu, G.-J. Cao and B. Chen, *ACS Appl. Mater. Interfaces*, 2022, **14**, 21098–21105.

62 P. Cui, E. Svensson Grape, P. R. Spackman, Y. Wu, R. Clowes, G. M. Day, A. K. Inge, M. A. Little and A. I. Cooper, *J. Am. Chem. Soc.*, 2020, **142**, 12743–12750.

63 Q. Yin, Y.-L. Li, L. Li, J. Lü, T.-F. Liu and R. Cao, *ACS Appl. Mater. Interfaces*, 2019, **11**, 17823–17827.

64 B. Yu, S. Geng, H. Wang, W. Zhou, Z. Zhang, B. Chen and J. Jiang, *Angew. Chem., Int. Ed.*, 2021, **60**, 25942–25948.

65 T. Takeda, M. Ozawa and T. Akutagawa, *Angew. Chem., Int. Ed.*, 2019, **58**, 10345–10352.

66 F. Hu, C. Liu, M. Wu, J. Pang, F. Jiang, D. Yuan and M. Hong, *Angew. Chem., Int. Ed.*, 2017, **56**, 2101–2104.

67 B. Wang, R. He, L.-H. Xie, Z.-J. Lin, X. Zhang, J. Wang, H. Huang, Z. Zhang, K. S. Schanze, J. Zhang, S. Xiang and B. Chen, *J. Am. Chem. Soc.*, 2020, **142**, 12478–12485.

68 J. H. Yoon, S. B. Choi, Y. J. Oh, M. J. Seo, Y. H. Jhon, T.-B. Lee, D. Kim, S. H. Choi and J. Kim, *Catal. Today*, 2007, **120**, 324–329.

69 S. Yuan, W. Lu, Y.-P. Chen, Q. Zhang, T.-F. Liu, D. Feng, X. Wang, J. Qin and H.-C. Zhou, *J. Am. Chem. Soc.*, 2015, **137**, 3177–3180.

70 P. Li, P. Li, M. R. Ryder, Z. Liu, C. L. Stern, O. K. Farha and J. F. Stoddart, *Angew. Chem., Int. Ed.*, 2019, **58**, 1664–1669.

71 X. Zhang, J.-X. Wang, L. Li, J. Pei, R. Krishna, H. Wu, W. Zhou, G. Qian, B. Chen and B. Li, *Angew. Chem., Int. Ed.*, 2021, **60**, 10304–10310.

72 P. Li, Z. Chen, M. R. Ryder, C. L. Stern, Q.-H. Guo, X. Wang, O. K. Farha and J. F. Stoddart, *J. Am. Chem. Soc.*, 2019, **141**, 12998–13002.

73 X. Zhang, L. Li, J.-X. Wang, H.-M. Wen, R. Krishna, H. Wu, W. Zhou, Z.-N. Chen, B. Li, G. Qian and B. Chen, *J. Am. Chem. Soc.*, 2020, **142**, 633–640.

74 J. Pang, S. Yuan, D. Du, C. Lollar, L. Zhang, M. Wu, D. Yuan, H.-C. Zhou and M. Hong, *Angew. Chem., Int. Ed.*, 2017, **56**, 14622–14626.

75 W. Liu, E. Wu, B. Yu, Z. Liu, K. Wang, D. Qi, B. Li and J. Jiang, *Angew. Chem., Int. Ed.*, 2023, **62**, e202305144.

76 W. Liu, K. Wang, X. Zhan, Z. Liu, X. Yang, Y. Jin, B. Yu, L. Gong, H. Wang, D. Qi, D. Yuan and J. Jiang, *J. Am. Chem. Soc.*, 2023, **145**, 8141–8149.

77 C. Bonneau, M. O'Keeffe, D. M. Proserpio, V. A. Blatov, S. R. Batten, S. A. Bourne, M. S. Lah, J.-G. Eon, S. T. Hyde, S. B. Wiggin and L. Öhrström, *Cryst. Growth Des.*, 2018, **18**, 3411–3418.

78 V. A. Blatov, A. P. Shevchenko and D. M. Proserpio, *Cryst. Growth Des.*, 2014, **14**, 3576–3586.

79 A. L. Spek, *Acta Crystallogr.*, 2009, **65**, 148–155.

80 Z. Wu, H. Choi and Z. M. Hudson, *Angew. Chem., Int. Ed.*, 2023, **62**, e202301186.

81 Y. Cui, T. Song, J. Yu, Y. Yang, Z. Wang and G. Qian, *Adv. Funct. Mater.*, 2015, **459**, 4796–4802.

82 Z. Hu, G. Huang, W. P. Lustig, F. Wang, H. Wang, S. J. Teat, D. Banerjee, D. Zhang and J. Li, *Chem. Commun.*, 2015, **51**, 3045–3048.

83 Y.-Y. Jia, J.-C. Yin, N. Li, Y.-H. Zhang, R. Feng, Z.-Q. Yao and X.-H. Bu, *Chin. J. Chem.*, 2021, **40**, 589–596.

84 N.-C. Chiu, K. T. Smith and K. C. Stylianou, *Coord. Chem. Rev.*, 2022, **459**, 214441.

85 Y.-X. Lin, J.-X. Wang, C.-C. Liang, C. Jiang, B. Li and G. Qian, *RSC Adv.*, 2022, **12**, 23411–23415.

86 Y. Lu, K. Yu, Q. Yin, J. Liu, X. Han, D. Zhao, T. Liu and C. Li, *Microporous Mesoporous Mater.*, 2022, **331**, 111673.

87 X.-H. Wu, Z. Wei, B.-J. Yan, R.-W. Huang, Y.-Y. Liu, K. Li, S.-Q. Zang and T. C. W. Mak, *CCS Chem.*, 2019, **1**, 553–560.

88 H.-T. Feng, X. Zheng, X. Gu, M. Chen, J. W. Y. Lam, X. Huang and B. Z. Tang, *Chem. Mater.*, 2018, **30**, 1285–1290.

89 P. Malakar, D. Modak and E. Prasad, *Chem. Commun.*, 2016, **52**, 4309–4312.

90 X.-Y. Liu, Y. Li, C.-K. Tsung and J. Li, *Chem. Commun.*, 2019, **55**, 10669–10672.

91 Z. Wang, C.-Y. Zhu, J.-T. Mo, P.-Y. Fu, Y.-W. Zhao, S.-Y. Yin, J.-J. Jiang, M. Pan and C.-Y. Su, *Angew. Chem., Int. Ed.*, 2019, **58**, 9752–9757.

92 S. Das, U. K. Ghorai, R. Dey, C. K. Ghosh and M. Pal, *Phys. Chem. Chem. Phys.*, 2017, **19**, 22995–23006.

93 M. Rai, G. Kaur, S. K. Singh and S. B. Rai, *Dalton Trans.*, 2015, **44**, 6184–6192.

94 M. Huang, Z. Liang, J. Huang, Y. Wen, Q.-L. Zhu and X. Wu, *ACS Appl. Mater. Interfaces*, 2023, **15**, 11131–11140.